**Palestine Journal of Mathematics**

**Vol 15(1)(2026)** , 425–444 

# MATHEMATICAL ANALYSIS OF SHEAR WAVE PROPAGATION IN A FLUID-SATURATED POROUS LAYER WITH INTERFACE IRREGULARITY

Ravinder Kumar, Suraj Sharma and Ananya Goyal

Communicated by: Geeta Arora

MSC 2020 Classifications: Primary 86A15; Secondary 74B10, 74J15.

Keywords: Anisotropy, shear waves, porosity, triangular irregularity, rigidity, phase velocity.

The authors sincerely thank the editor and reviewers for their helpful feedback and insightful suggestions that enhanced the overall quality of the manuscript.

Corresponding Author: Ravinder Kumar

**Abstract** This study examines shear-wave propagation in a transversely isotropic fluid saturated porous layer (TIFSPL) of finite height $H$, with a rigid upper surface at $z = -H$ and lying above heterogeneous elastic half-space, with a continuous interface at $z = \epsilon h(x)$ representing a triangular irregularity. Analytical dispersion relation is derived using poroelasticity theory by Biot, Fourier transform techniques, and first-order perturbation for small irregularity amplitude $\epsilon$. Numerical simulations performed using MATLAB explore the influence of porosity, inhomogeneity parameter, anisotropy factor, and the irregularity depth to the layer height ratio on phase velocity. The results show that phase velocity rises with increasing anisotropy and with a higher ratio of irregularity depth to layer height, but decreases with porosity and material inhomogeneity. The combined parameter interactions and crossings of dispersion branches are discussed, providing useful insights into shear-wave behavior in complex porous media.

## 1 Introduction

Seismology, the study of the earthquakes and the seismic waves, plays a vital role in understanding Earth's structure and assessing earthquake risks. It has numerous applications across various disciplines, including civil engineering, geophysics, structural engineering, seismic hazard analysis, and rock mechanics. By analyzing seismic wave frequency, magnitude, and location, researchers can generate detailed images of Earth's interior and gain insights into its dynamic processes. The detailed literature on seismology, earthquakes, seismic waves, and related terminology is available from sources such as Biot [1-2], Kończak [3], Shearer [4], and Gubbins [5]. The propagation of seismic waves through layered media has been extensively studied, as understanding these wave movements is crucial for advancements in geophysics and seismology. Studying seismic wave motion in elastic layers is valuable since it has many practical uses in areas such as soil mechanics, earthquake engineering, and geophysical exploration. Seismic waves are generated when there is a rupture or movement along a fault line, releasing energy that radiates outward from the earthquake's epicentre. Among seismic waves, shear waves have attracted significant attention due to their unique characteristics and practical applications. Shear waves, also called secondary waves, travel through solid materials, make the particles of the medium to oscillate perpendicular to the wave propagation direction. The purely horizontal particle motion of shear waves makes their mathematical treatment simple while preserving their diagnostic potential. These waves are especially significant in applications such as earthquake hazard analysis, subsurface imaging, and non-destructive material testing. These are extremely useful for examining intricate geological systems because of their sensitivity to changes in material characteristics, layer thickness, and subsurface irregularities. Research on Love waves began with foundational work by Love [6], who first described shear horizontal wave behavior in an

isotropic homogeneous elastic layer over a semi-infinite substrate. Ewing et al. [7] extended this understanding by analyzing surface waves in elastic media, emphasizing the importance of layer thickness and substrate rigidity on wave velocity. Graff [8] provided a comprehensive treatment of wave propagation in elastic solids, illustrating how dispersion relations for Love waves vary with frequency. Achenbach [9] focused on elasto-dynamics wave theory, introducing the influence of multiple layers on surface wave characteristics. Chattopadhyay and Kar [10] used Green's function to study the propagation of Love-type surface waves from a point source in an elastic isotropic material under initial stress. The main focus of the classical studies on seismic wave propagation are on simple, homogeneous, and isotropic elastic media. Real-world scenarios, on the other hand, are much more complicated and frequently involve elements like anisotropy, irregular surface geometry, thermoelastic effects, and material inhomogeneity. Understanding how waves propagate in non-homogeneous media, where material characteristics like density, elasticity, or thermal conductivity vary with position is crucial to comprehending systems in the real world. These variations create complexities that significantly impact wave behavior, especially in terms of dispersion, where different wave frequencies travel at different speeds. Geological materials often exhibit anisotropy, where their physical properties differ depending on the direction. A specific form of anisotropy, known as transverse isotropy, is observed in materials with a single axis of symmetry. This concept helps explain geological formations such as sedimentary rock layers, the Earth's internal structure. The presence of interface irregularities is also one of the most significant factors that can alter the characteristics of shear waves. These irregularities such as depressions, or discontinuities have a profound influence on seismic wave propagation behavior. The presence of the irregularities at the interface complicates the behavior of seismic waves, which are important in both earthquake analysis and material testing. Understanding these effects has been a primary focus for seismologists and researchers, who have developed various models and methodologies to explain how irregularities, in combination with other factors, influence seismic wave propagation. Regarding Fourier transformation and perturbation techniques, Eringens pioneered methods for solving complex boundary-value problems in wave mechanics. These mathematical approaches have been effectively applied in analyzing wave dispersion relations, particularly in layered media with elastic and poroelastic properties. In the context of numerical simulations, MATLAB based approaches have been widely used to visualize dispersion relations and interpret wave behavior in complex systems.

Various studies have examined seismic wave propagation behavior in diverse media with irregular boundaries and interface irregularities. For example, Dutta et al. [11] analyzed the behavior of seismic wave propagation on irregular structures, while Chattopadhyay et al. [12] investigated shear wave movement through irregular magnetoelastic monoclinic layers situated between half spaces. Chattopadhyay et al. [13] analyzed shear wave behavior in viscoelastic media with irregular boundaries. Alam et al. [14] derived the dispersion relation for SH-waves in crystal layers situated above irregular half-spaces, while the study by Kaur et al. [15] examined the effect of irregular geologies and inhomogeneities on horizontally polarized shear wave movement. Wang and Zang [16] provides the examination of Love waves in a TIFSPL medium. This study describes surface waves through the summation of plane waves, offering a foundational approach to analyzing wave behavior in anisotropic materials. Gupta et al. [17] explored how irregularities affect Love wave movement through porous layers considering rigidity factors. Kundu et al. [18] examined Love waves in porous layers situated above initially stressed half-spaces. Kumar and Saini [19] studied the role of parabolic irregularity, material inhomogeneity, and initial stress on Love wave behavior in elastic layers with pores. Kumar et al. [20] focused on how irregularities and inhomogeneities impact Love wave propagation in FSPL (fluid saturated porous layers). Manna et al. [21] looked into the effects of reinforcement and inhomogeneity on Love waves. Kumar et al. [22] studied shear wave movement in irregular FSPL. Saini and Kumar [23] analyzed Love wave behavior in porous layers over heterogeneous half-spaces with parabolic-shaped irregularity. Recent advancements have focused on the interaction of shear waves with complex geological structures. Numerous researchers have also studied the influence of various parameters affecting the movement of shear waves by considering different geophysical models. Chattopadhyay et al. [24] has studied the influence of irregularity and anisotropy on shear wave movement. Samal et al. [25] studied the propagation of shear waves in an anisotropic elastic layer reinforced with fibres, situated between a porous half space and a uniform liquid layer.

Kumar et al. [26] investigated propagation of shear wave in a multilayered medium, encompassing an irregular FSPL with a rigid boundary. Kundu et al. [27] formulated the dispersion relation for shear waves with horizontal polarization in an isotropic medium situated between orthotropic and non-uniform half-space, while Kundu et al. [28] examined shear waves within a magnoelastic layer positioned between two diverse elastic media. Gupta et al. [29] has shown the impact of factors such as irregularity, porosity, and initial stress on SH-wave propagation. Kumar et al. [30] studied the behavior of shear waves in an anisotropic porous layer showing how anisotropy, heterogeneity, and irregularity influence wave dispersion. Sharma and Kumar [31] analyzed shear horizontal wave propagation in a multilayered system where a transversely isotropic fluid-saturated porous layer is placed between a homogeneous layer and a non-homogeneous elastic half-space. Poonia et al. [32] formulated the dispersive equation and examined the influence of irregularity, rigidity and initial stress on SH-wave movement. Kumar and Saini [33] explored the effects of porosity, parabolic-shaped irregularities, and initial stress in multi-layered systems and showed how these factors affect the dispersion relation of seismic waves. Several other researchers have contributed to this field, including Sharma and Kumar [34], Saini and Kumar [35], Gaba et al. [36], and Singh et al. [37]. This research aims to fill the identified gap by formulating a detailed model that incorporates multiple influencing factors to better represent shear wave behavior in layered geological structures.

The primary objective is to analyze how triangular-shaped irregularities, material rigidity, heterogeneity, porosity and initial stress affect the propagation of shear waves in a porous layer positioned above a heterogeneous elastic half-space. This manuscript is structured into several sections. Section 2 elaborates on the considered model, comprising two mediums, $M1$ and $M2$ with a rigid boundary, and defines the equation of irregularity. In Section 3, the fundamental governing equation for the porous layer and half space, utilizing Biot's elastic theory has been discussed. Section 4 addresses the determination of appropriate boundary conditions for the model, followed by the solution of the basic equations using boundary conditions, perturbation methods, and Fourier transformation techniques in Sections $5-7$. In Section 8, the graphical numerical results for shear waves using MATLAB have been presented. The non-dimensional phase velocity is plotted in relation to non-dimensional wavenumber for the different values of the inhomogeneity parameter, anisotropy factor and porosity considering different ratios of irregularity depth to layer's height. The derived dispersion equation in Section 8 shows the relationship between wavenumber, phase velocity, porosity, anisotropy factor, depth of irregularity and the layer. Finally, section 9 offers conclusions from the study, followed by a list of references cited throughout the paper.

## 2 Mathematical Formulation of the Problem

Consider a TIFSPL (defined as medium $M1$) of finite thickness $H$ resting over a heterogeneous elastic half-space (defined as medium $M2$). The upper surface of TIFSPL is assumed to be rigid, while the interface separating the layer and the half-space is assumed to be continuous and with triangular shaped irregularity. The $z$-axis is directed vertically downward, and $x$-axis is taken along the mean horizontal interface, as shown in Fig.1. The origin of the coordinate system is located on the mean interface, and the equation of the irregular interface is represented as $z = \epsilon h(x)$, where $\epsilon$ $(\epsilon \ll 1)$ is considered a small dimensionless perturbation parameter representing the amplitude of the triangular irregularity relative to the layer thickness, and $h(x)$ is a known function that defines the shape of the irregular interface.
For a triangular-shaped irregularity, the surface profile can be represented as

$$h(x) = \begin{cases} 0, & \text{for } |x| \geq s \\ 2s(1 - \frac{x}{s}), & \text{for } 0 < x < s \\ 2s(1 + \frac{x}{s}), & \text{for } -s < x < 0 \end{cases} \tag{2.1}$$

where $2s$ denotes the base width of the triangular irregularity and $l_1$ is its height. The ratio $\epsilon = \dfrac{l_1}{2s}$ serves as the perturbation parameter in the analysis. The region $-H \leq z \leq \epsilon h(x)$ cor-

responds to the fluid-saturated porous layer, and the region $z \geq \epsilon h(x)$ represents the underlying heterogeneous elastic half-space.

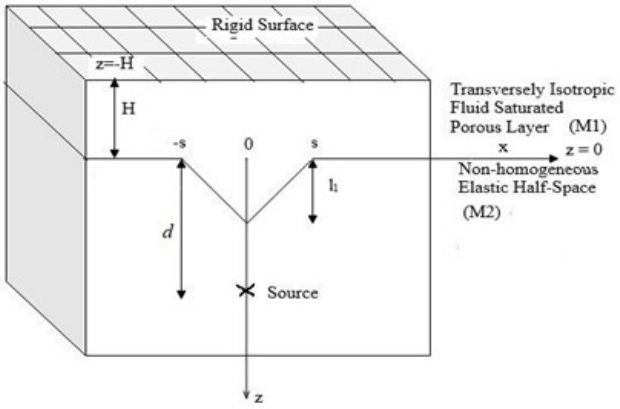


**Figure 1.** Mathematical Model of the Problem

## 3 Basic Equations

The key equations for both Mediums, that define the model are provided below.

According to Biot [1], the equations of motion for medium M1, excluding body forces, are

$$\begin{aligned} \sigma_{ij,j} &= \rho_{11}\ddot{u}_i + \rho_{12}\ddot{U}_i - b_{ij}(\dot{U}_j - \dot{u}_j), \\ \sigma_{,i} &= \rho_{12}\ddot{u}_i + \rho_{22}\ddot{U}_i + b_{ij}(\dot{U}_j - \dot{u}_j). \end{aligned} \tag{3.1}$$

Here, the comma indicates differentiation in terms of position, while the dot represents differentiation in terms of time.

Biot's formulation for the porous structure, established a relationship and explained that the mass coefficients $(\rho_{11}, \rho_{12}, \text{and } \rho_{22})$ are connected to total mass density $\rho$ for the solid and liquid mixture, as well as the individual mass densities $\rho_s$ and $\rho_\phi$ as

$$\begin{aligned} \rho_{11} + \rho_{12} &= (1-\phi)\rho_s, \\ \rho_{12} + \rho_{22} &= \phi\rho_\phi, \\ \rho &= \rho_s + \phi(\rho_f - \rho_s). \end{aligned} \tag{3.2}$$

The stress and strain relationship for medium M1 is presented as

$$\begin{aligned} \sigma_{11}^{(1)} &= (2C_1 + C_2)e_{11} + C_2 e_{22} + C_3 e_{33} + C_6 E, \\ \sigma_{22}^{(1)} &= C_2 e_{11} + (2C_1 + C_2)e_{22} + C_3 e_{33} + C_6 E, \\ \sigma_{33}^{(1)} &= C_3 e_{11} + C_3 e_{22} + 2C_4 e_{33} + C_7 E, \\ \sigma_{23}^{(1)} &= 2C_5 e_{23}, \\ \sigma_{31}^{(1)} &= 2C_5 e_{31}, \\ \sigma_{12}^{(1)} &= 2C_1 e_{12}, \\ \sigma^{(1)} &= C_6 e_{11} + C_6 e_{22} + C_7 e_{33} + C_8 E. \end{aligned} \tag{3.3}$$

where

$$\begin{aligned} E &= \text{div}U = U_{j,j}, \\ e &= \text{div}u = u_{k,k}, \\ e_{ij} &= \frac{1}{2}(u_{i,j} + u_{j,i}). \end{aligned} \tag{3.4}$$

As the shear waves travel with the $x$-axis, the resulting displacement will occur in the trajectory of the $z$-axis, allowing us to assume that:

$$\begin{aligned} u_1 = 0, \quad u_2 = u_2(x,z,t), \quad u_3 = 0, \\ U_1 = 0, \quad U_2 = U_2(x,z,t), \quad U_3 = 0. \end{aligned} \tag{3.5}$$

On solving equation (3.1) with the help of equations (3.3)-(3.5), yields that:

$$\begin{aligned} \frac{\partial^2}{\partial t^2}(\rho_{12}u_2 + \rho_{22}U_2) + b_{11}\frac{\partial}{\partial t}(U_2 - u_2) = 0, \\ C_1\frac{\partial^2 u_2}{\partial x^2} + C_5\frac{\partial^2 u_2}{\partial z^2} = \frac{\partial^2}{\partial t^2}(\rho_{11}u_2 + \rho_{12}U_2) - b_{11}\frac{\partial}{\partial t}(U_2 - u_2). \end{aligned} \tag{3.6}$$

Rewriting equation (3.6) by removing $u_2$ and $U_2$, yields that:

$$\left\{ C_1\frac{\partial^2}{\partial x^2} + C_5\frac{\partial^2}{\partial z^2} - \left[\rho_{11}\partial_t^2 + b_{11}\partial_t - \frac{(\rho_{12}\partial_t^2 - b_{11}\partial_t)^2}{\rho_{22}\partial_t^2 + b_{11}\partial_t}\right](u_2, U_2) = 0. \right. \tag{3.7}$$

The equations of motion for medium M2, excluding body forces, as outlined by Konczak [3], are:

$$\tau_{ij,j} = \rho\ddot{v}_i. \tag{3.8}$$

The constitutive relations are given by:

$$\tau_{ij} = \lambda e_{kk}\delta_{ij} + 2\mu e_{ij}, \tag{3.9}$$

$$\begin{aligned} 2e_{ij} = (v_{i,j} + v_{j,i}), \\ e_{kk} = v_{k,k} = e. \end{aligned} \tag{3.10}$$

Using (3.9) and (3.10), the equation (3.8) is rewritten as:

$$[(\lambda + 2\mu)^* e] - 2\mu_i e - \mu e_{,j} + \mu v_{i,jj} + \mu_{,}j(v_{i,j} + v_{j,i}) = \rho\ddot{v}_i. \tag{3.11}$$

Considering the shear waves travelling in the direction along the $x$-axis, yields that $v_1 = 0, v_2 = v_2(x,z,t), v_3 = 0$, and thus, equation (3.11) is reduced to:

$$\left(\frac{\partial^2}{\partial x^2} + \frac{\partial^2}{\partial z^2}\right)v_2 = \frac{1}{\beta^2}\frac{\partial^2 v_2}{\partial t^2}. \tag{3.12}$$

The material parameters of the lower half-space are considered to vary exponentially with depth according to

$$\mu = \mu_0 e^{qz}, \qquad \rho = \rho_0 e^{qz}, \tag{3.13}$$

where $\mu_0$ and $\rho_0$ are reference values of shear modulus and density at the interface, respectively, and $q$ is the inhomogeneity parameter. The exponential model is adopted because it preserves positive material properties, realistically represents gradual stratification, and facilitates analytical treatment through Fourier transforms.

## 4 Boundary Conditions

The applicable boundary conditions for the deliberated problem are mentioned as below:

(i) Because of rigid surface at $z = -H$, the component of displacement becomes null, i.e.,

$$u_2(x, -H, t) = 0. \tag{4.1}$$

(ii) At the interface $z = \epsilon h(x)$, the displacements are continuous, i.e.,

$$u_2(x, -H, t) = v_2(x, -H, t). \tag{4.2}$$

(iii) At the interface $z = \epsilon h(x)$, the stresses also remain continuous, meaning that:

$$C_5\frac{\partial u_2}{\partial z}\Big|_{z=\epsilon h(x)} - C_1\epsilon h'(x)\frac{\partial u_2}{\partial x}\Big|_{z=\epsilon h(x)} = \mu_0\Big(\frac{\partial v_2}{\partial z}\Big|_{z=\epsilon h(x)} - \epsilon h'(x)\frac{\partial v_2}{\partial x}\Big|_{z=\epsilon h(x)}\Big). \tag{4.3}$$

where, $h'(x)$ represents the one-time differentiation of $h(x)$ with respect to $x$.

## 5 Analytical Solution of the Problem

For waves travelling in the $x$ direction and oscillating periodically with $t$ time within mediums M1 and M2, the assumptions applied to the displacement vectors are as:

$$\begin{aligned} u_2(x,z,t) &= u_2^0(x,z)e^{i\omega t}, \\ U_2(x,z,t) &= U_2^0(x,z)e^{i\omega t}, \\ v_2(x,z,t) &= v_2^0(x,z)e^{i\omega t}. \end{aligned} \tag{5.1}$$

Now, by taking equation (5.1) in (3.7), it simplifies to:

$$\left\{ C_1 \frac{\partial^2}{\partial x^2} + C_5 \frac{\partial^2}{\partial z^2} + \zeta_1^2 \right\} (\dot{u}_2^0, U_2^0) = 0. \tag{5.2}$$

where $\zeta_1^2 = \alpha_1 + i\alpha_2$, $\alpha_1$ and $\alpha_2$ are defined in appendix (A).
Using equation (5.1), equation (3.12) converts into the form:

$$\left\{ \frac{\partial^2}{\partial x^2} + \frac{\partial^2}{\partial z^2} + q\frac{\partial}{\partial z} + \frac{\omega^2}{\beta^2} \right\} v_2^0 = 0. \tag{5.3}$$

Using Fourier transformation which is given in appendix section (A), the equation (5.2) and (5.3) yields:

$$\begin{aligned} \frac{\partial^2 u_2^0}{\partial z^2} + \chi_1^2 u_2^0 &= 0, \\ \frac{\partial^2 U_2^0}{\partial z^2} + \chi_1^2 U_2^0 &= 0, \\ \frac{\partial^2 v_2^0}{\partial z^2} - \chi^2 v_2^0 &= 0. \end{aligned} \tag{5.4}$$

where $\chi_1^2$ and $\chi^2$ are defined in appendix section (A). The solutions of equation (5.4) are:

$$\begin{aligned} u_2^0 &= A_{11}\cos\chi_1 z + A_{22}\sin\chi_1 z, \\ U_2^0 &= \overline{A_{11}}\cos\chi_1 z + \overline{A_{22}}\sin\chi_1 z, \\ v_2^0 &= A_{33}\exp(-\chi z). \end{aligned} \tag{5.5}$$

As, $A_{11}, A_{22}, \overline{A_{11}}, \overline{A_{22}}$ and $A_{33}$ are the function of $\eta$, and by applying inverse Fourier transformation defined in appendix section on equation (5.5), yields that:

$$\begin{aligned} u_2^0(x,z) &= \frac{1}{2\pi}\int_{-\infty}^{\infty} (A_{11}\cos\chi_1 z + A_{22}\sin\chi_1 z)e^{-i\eta x}d\eta, \\ U_2^0(x,z) &= \frac{1}{2\pi}\int_{-\infty}^{\infty} (\overline{A_{11}}\cos\chi_1 z + \overline{A_{22}}\sin\chi_1 z)e^{-i\eta x}d\eta, \end{aligned} \tag{5.6}$$

$$v_2^0(x,z) = \frac{1}{2\pi}\int_{-\infty}^{\infty} A_{33}\exp(-\chi z)e^{-i\eta x}d\eta. \tag{5.7}$$

Thus, from the equation (5.7), the displacement vector for medium M2 becomes:

$$v_2^0(x,z) = \frac{1}{2\pi}\int_{-\infty}^{\infty} (A_{33}\exp(-\chi z) + \frac{2}{\chi}e^{\chi z}e^{-\chi d})e^{-i\eta x}d\eta. \tag{5.8}$$

The inclusion of an irregularity in the medium M2 leads to the addition of a new expression on the right side of equation (5.8).

## 6 Methodology for Solving the Problem

The perturbation method is employed to address the mathematical complexity arising from the triangular-shaped interface irregularity and its associated boundary conditions. A small, dimensionless parameter $\varepsilon$ is introduced to represent the amplitude of the irregularity. The displacement field is expanded in powers of $\varepsilon$ to obtain a systematic and controlled approximation of the governing equations. In this analysis, it is explicitly assumed that $\varepsilon \ll 1$, and all terms of order $\varepsilon^2$ and higher are neglected. This assumption ensures that the derived dispersion relation accurately represents the leading-order effects of the interface geometry on shear wave propagation.

The following approximations are applied:

$$A_{11} \cong A_1 + \epsilon A_1^0, \quad A_{22} \cong A_2 + \epsilon A_2^0, \quad A_{33} \cong A_3 + \epsilon A_3^0, \tag{6.1}$$

$$e^{\pm a\epsilon h} \cong 1 \pm a\epsilon h, \quad \cos\chi_i eh \cong 1, \quad \sin\chi_i eh \cong \chi_i eh. \tag{6.2}$$

Using equations (6.1) and (6.2), the applicable boundary conditions (4.1) - (4.3) yield:

$$(A_1 + \epsilon A_1^0)\cos\chi_1 H - (A_2 + \epsilon A_2^0)\sin\chi_1 H = 0, \tag{6.3}$$

$$(A_1 + \epsilon A_1^0)\cos\chi_1\epsilon h + (A_2 + \epsilon A_2^0)\sin\chi_i\epsilon h = (A_3 + \epsilon A_3^0)e^{-\chi\epsilon h(x)} + \frac{2}{\chi}e^{-\chi\epsilon h(x)}e^{-\chi d}, \tag{6.4}$$

$$\begin{aligned} C_s\chi_1[A_2 + \epsilon A_2^0 - \epsilon A_1\chi_1 h(x)] + \iota\eta C_1\epsilon h'(x)A_1 = \\ \mu_0\left[-\chi A_3 + A_3\chi^2\epsilon h(x) - \chi\epsilon A_3^0 + 2e^{-\chi d} + 2\epsilon\chi h(x)e^{-\chi d} + \epsilon\iota\eta h'(x)\left(A_3 + \frac{2}{\chi}e^{-\chi d}\right)\right]. \end{aligned} \tag{6.5}$$

Equating the terms independent of $\epsilon$ and the coefficients of $\epsilon$, isolate the coefficients of the function $h'(x)$ and $h(x)$ from equations (6.3) - (6.5) gives:

$$\begin{aligned} A_1\cos\chi_1 H - A_2\sin\chi_1 H &= 0, \\ A_1^0\cos\chi_1 H - A_2^0\sin\chi_1 H &= 0, \\ A_1 - A_3 &= \frac{2}{\chi}e^{-\chi d}, \\ A_3^0 - A_1^0 &= E_1(k), \\ C_5\chi_1 A_2 + \mu_0\chi A_3 &= 2\mu_0 e^{-\chi d}, \\ \chi_1 C_5 A_2^0 + \mu_0\chi A_3^0 &= E_2(k). \end{aligned} \tag{6.6}$$

where $A_1, A_1^0, A_2, A_2^0, A_3, A_3^0$ and $E_1(k), E_2(k)$ are defined in appendix. Thus, the displacement vector in equation (5.6) becomes:

$$\begin{aligned} u_2^0(z,x) = \frac{1}{2\pi}\int_{-\infty}^{\infty}\left(\frac{4\mu_0 e^{-\chi d}}{E(k)}\right)\left[1 + \frac{\epsilon(E_2(k) - \mu_0\chi E_1(k))e^{\chi d}}{4\mu_0}\right] \\ (\cos\chi_1 z - \tan\chi_1 H\sin\chi_1 z)e^{-ikx}\,dk. \end{aligned} \tag{6.7}$$

Now, from the equations (2.1) and (2.2) and with the help of appendix (B), yields that:

$$\bar{h}(\lambda) = \frac{2s}{\lambda^2}\sin^2(\lambda s). \tag{6.8}$$

Using the expressions $E_1(k)$ and $E_2(k)$ as given in appendix (B), yields:

$$E_2 - \mu_0\chi E_1 = \frac{2s\mu_0}{\pi}\int_{-\infty}^{\infty}(g(k-\lambda) + g(k+\lambda))\,\frac{1}{\lambda^2}\sin^2(\lambda s)d\lambda. \tag{6.9}$$

where $g(k-\lambda) = B_2 + B_3$, $B_2$ and $B_3$ are defined in appendix section (B).

By applying asymptotic formula given by Willis [38] and disregarding the terms with the highest power of $2/s$, due to large value of $s$, obtained that:

$$\int_{-\infty}^{\infty} [g(k-\lambda)+g(k+\lambda)]\,\frac{1}{\lambda^2}\sin^2(\lambda s)d\lambda = \frac{\pi}{2}g(k) = \pi g(k). \tag{6.10}$$

Now, equation (6.9) with the help of equation (6.10) gives:

$$E_2 - \mu_0\chi E_1 = s\mu_0 g(k) = \mu_0\frac{l_1}{2\epsilon}g(k). \tag{6.11}$$

Therefore, the displacement equation (6.7) becomes

$$u_2^0 = \frac{1}{2\pi}\int_{-\infty}^{\infty} \frac{4\mu_0 e^{-\chi d}}{R(k)\left[1-\frac{l_1}{2}g(k)e^{\chi d}\right]}(\cos\chi_1 z - \tan\chi_1 H\sin\chi_1 z)e^{-kx}\,dk. \tag{6.12}$$

The displacement vector within the layer is determined by the contributions from the poles of the equation (6.12)

$$R(K)\left[1-\frac{l_1}{2}y(k)e^{\chi d}\right] = 0. \tag{6.13}$$

where $y(k)$ is defined in appendix section (B).

## 7 Complex Dispersion Relation

On solving equation (6.13), we have

$$\tan\chi_1 H = \frac{C_5\chi_1(1-2l_1\chi)+2l_1\mu_0\chi_1\chi}{2l_1(C_5\chi_1^2+\mu_0\chi^2)+\mu_0\chi}. \tag{7.1}$$

Substituting $\omega = ck$, $\chi_1 = P_1 k$, $q = Qk$, and $\chi = P_2 k$ defined in appendix (A), the equation (7.1) converts to

$$\tan P_1 kH = \frac{\mu_0 P_2 k - 4l_1(C_5 P_1^2 k + \mu_0 P_2^2 k)}{C_5 P_1 + 4l_1 P_2 P_1 k(\mu_0 - C_5)}. \tag{7.2}$$

where

$$P_1 = k_1 + \iota k_2. \tag{7.3}$$

$P_1$, $P_2$, $k_1$ and $k_2$ are listed in appendix section C.
By using equation (7.3), the dispersion equation (7.1) becomes

$$\tan(k_1+\iota k_2)kH = L_r + \iota L_i \tag{7.4}$$

where $L_r$ and $L_i$ are defined in appendix section C.
Consider $k_2$ as very small, gives

$$\tan(k_1+\iota k_2)kH = \frac{\tan(k_1 kH + \iota k_2 kH)}{1-\iota(k_2 kH)\tan(k_1 kH)}. \tag{7.5}$$

Hence, using equations (7.5) with the help of appendix (C), two real equations obtained

$$\begin{aligned} \tan(k_1 kH) &= \frac{L_r}{1-L_i(k_2 kH)}, \\ k_2 kH(l+L_r, \tan(k_1 kH)) &= L_i. \end{aligned} \tag{7.6}$$

As a result, the dispersion equation for shear waves comprises the real part of equation (7.6), i.e.

$$\tan(k_1 kH) = L_r(1+L_i k_2 kH). \tag{7.7}$$

## 8 Analysis and Interpretation of Numerical Results

This section shows the graphical and numerical analysis of the dispersion equation associated with shear wave movement in a porous layer with a upper rigid boundary, placed over a heterogeneous half-space. The effects of porosity, anisotropy, heterogeneity, and triangular irregularity are examined. The relationship between the non-dimensional phase velocity and the non-dimensional wavenumber for various parameters is explored using MATLAB and graphical routines have been plotted. For this purpose, the data for both mediums has been taken from Kończak [3], and Gubbins [5], and given as under:

**Table 1.** Standard parameter set used in numerical computations.

| Symbol | Meaning | Value | Units | Remarks |
|---|---|---|---|---|
| $\mu_0$ | Shear modulus of half-space | $7.10 \times 10^{10}$ | $\mathrm{N\,m^{-2}}$ | Dimensional |
| $C_5$ | Shear modulus in layer | $0.2765 \times 10^{10}$ | $\mathrm{N\,m^{-2}}$ | Dimensional |
| $\mu/C_5$ | Shear modulus ratio | 4 | – | Non-dimensional |
| $\beta$ | Shear wave speed | 3600 | $\mathrm{m\,s^{-1}}$ | Fixed |
| $\omega$ | Angular frequency | 40000 | $\mathrm{s^{-1}}$ | Fixed |
| $\gamma_{11}$ | $\rho_{11}/\rho$ | 0.666 | – | Numerical |
| $\gamma_{12}$ | $\rho_{12}/\rho$ | 0 | – | Coupling neglected |
| $\gamma_{22}$ | $\rho_{22}/\rho$ | 0.333 | – | Numerical |
| $f$ | Porosity-related factor | 0.25 | – | – |
| $H$ | Layer height | 1.0 | m (normalized) | – |
| $l_1/H$ | Irregularity depth ratio | 0.10–0.30 | – | Variable |
| $q$ | Inhomogeneity parameter | 0–3 | – | Variable |
| $D_1$ | Non-dimensional porosity parameter | 0.6–0.9 | – | $D_1 = 1 - \phi$ |
| $\phi$ | Physical porosity | 0.4–0.1 | – | – |

By using these values, the behavior of non-dimensional phase velocity versus non-dimensional wavenumber has been graphically shown for various values of the non-homogeneous parameter $q$, anisotropic factor $C_1/C_5$, porosity parameter (represented by $D$), and the ratio $l_1/H$. The results have been plotted as follows:

Figures 2-5 illustrate how the non-dimensional phase velocity varies with the non-dimensional wavenumber for distinct values of the inhomogeneity parameter ($q = 0, 1, 2, 3$) and the ratio ($l_1/H = 0.10, 0.15, 0.20, 0.25$, and $0.30$). The figures show that as the ratio $\frac{l_1}{H}$ increases, the phase velocity increases accordingly. Conversely, an increment in the inhomogeneity parameter $q$ lowers the phase velocity.

Figures 6-9 show how the non-dimensional phase velocity changes with non-dimensional wave number, examining the impact of the anisotropy factor $\frac{C_1}{C_5} = 1, 2$ for two scenarios: one where the half space medium is homogeneous ($q = 0$) and one where it is non-homogeneous ($q = 1$). The analysis considers various values of the ratio ($\frac{l_1}{H} = 0.10, 0.15, 0.20, 0.25$, and $0.30$). The comparison of the curves shows that an increase in the anisotropy factor leads to higher phase velocities, while a rise in the inhomogeneity parameter results in lower phase velocities.

Figures 10-13 illustrate the plots showing how the non-dimensional phase velocity varies with the non-dimensional wavenumber for various porosity values ($D = 0.6, 0.7, 0.8, 0.9$) and the ratios $\frac{l_1}{H} = 0.10, 0.15, 0.20, 0.25$. These plots have been illustrated that an increment in the porosity factor $(D)$ leads to a decrement in phase velocity and with an increment in the values of the ratio $(\frac{l_1}{H})$, the phase velocity increases.

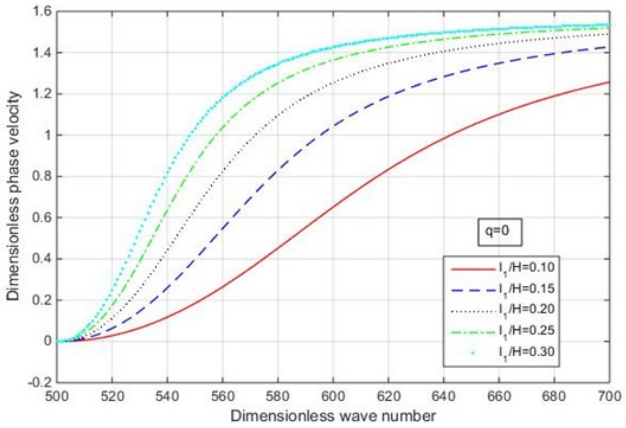


**Figure 2.** Dispersion curves for the ratios $\frac{l_1}{H} = 0.10, 0.15, 0.20, 0.25$, and 0.30 and the inhomogeneity parameter $q = 0$ .

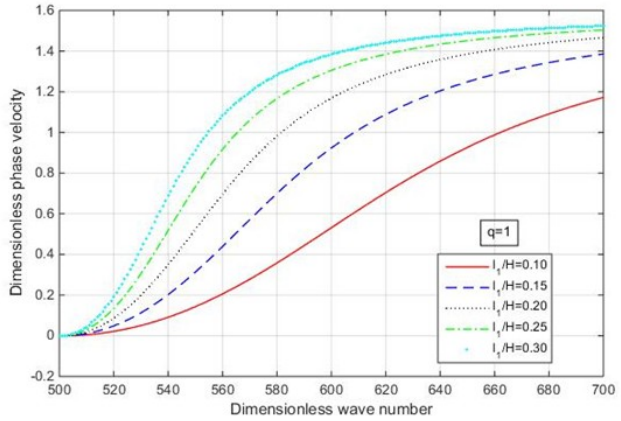


**Figure 3.** Dispersion curves for the ratios $\frac{l_1}{H} = 0.10, 0.15, 0.20, 0.25$, and 0.30 and the inhomogeneity parameter $q = 1$ .

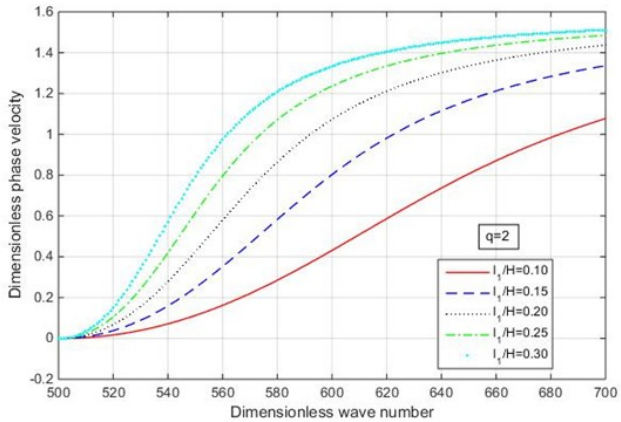


**Figure 4.** Dispersion curves for the ratios $\frac{l_1}{H} = 0.10, 0.15, 0.20, 0.25$, and 0.30 and the inhomogeneity parameter $q = 2$ .

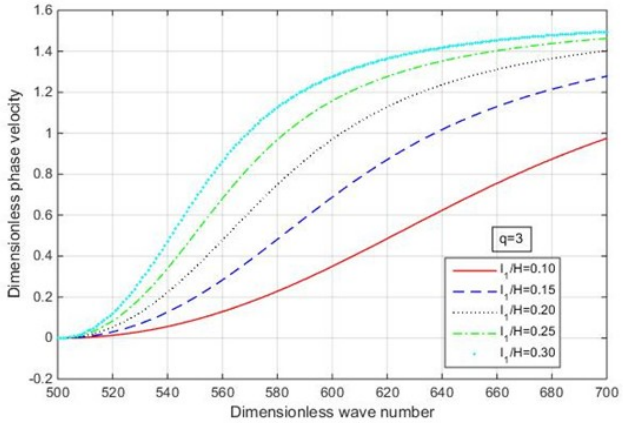


**Figure 5.** Dispersion curves for the ratios $\frac{l_1}{H} = 0.10, 0.15, 0.20, 0.25$, and 0.30 and the inhomogeneity parameter $q = 3$ .

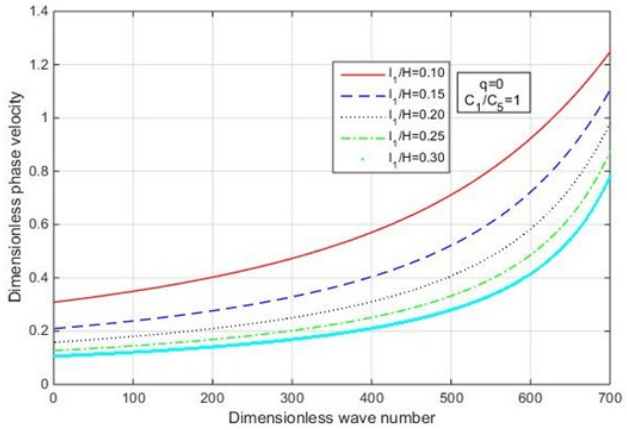


**Figure 6.** Impact of the anisotropy factor $\frac{C_1}{C_5} = 1$ on dispersion curves for $\frac{l_1}{H} = 0.10, 0.15, 0.20, 0.25$, and 0.30 in case of lower non-homogeneous half space medium.

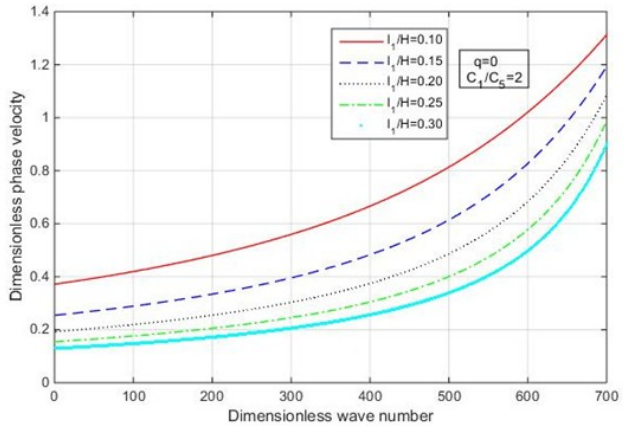


**Figure 7.** Impact of the anisotropy factor $\frac{C_1}{C_5} = 2$ on dispersion curves for $\frac{l_1}{H} = 0.10, 0.15, 0.20, 0.25$, and 0.30 in case of lower non-homogeneous half space medium.

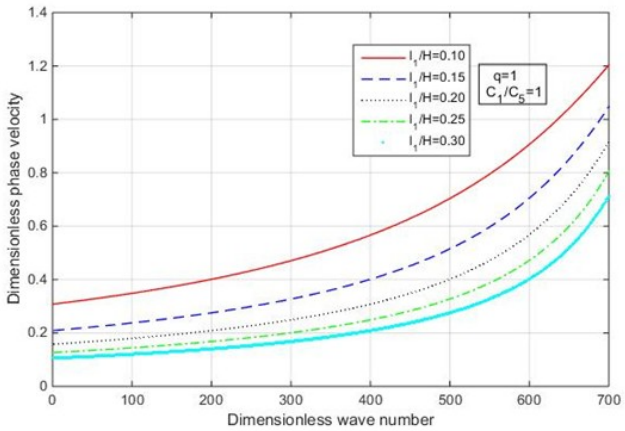


**Figure 8.** Impact of the anisotropy factor $\frac{C_1}{C_5} = 1$ on dispersion curves for $\frac{l_1}{H} = 0.10, 0.15, 0.20, 0.25$, and 0.30 in case of lower non-homogeneous half space medium.

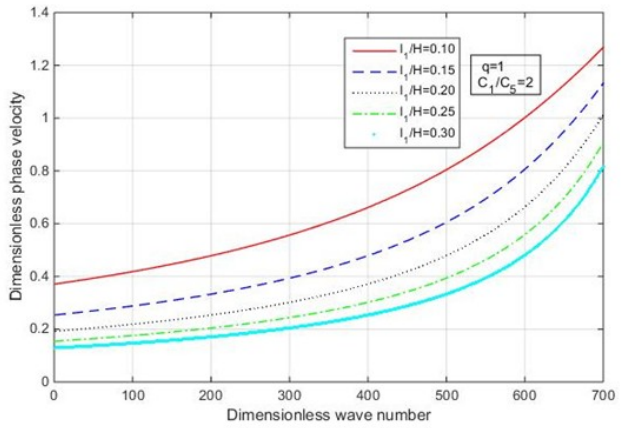


**Figure 9.** Impact of the anisotropy factor $\frac{C_1}{C_5} = 2$ on dispersion curves for $\frac{l_1}{H} = 0.10, 0.15, 0.20, 0.25$, and 0.30 in case of lower non-homogeneous half space medium.

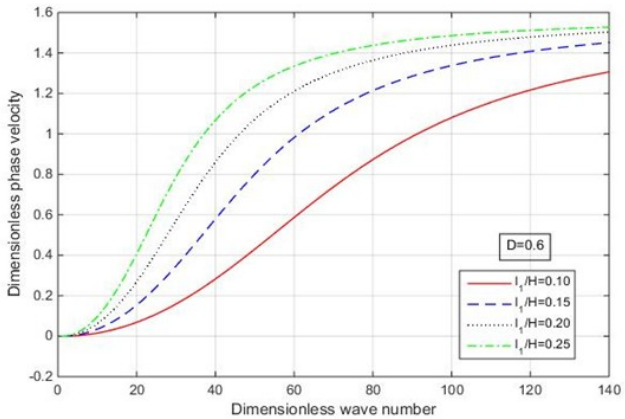


**Figure 10.** Dispersion curves for porosity factor $D = 0.6$ and the ratios $\frac{l_1}{H} = 0.10, 0.15, 0.20, 0.25$.

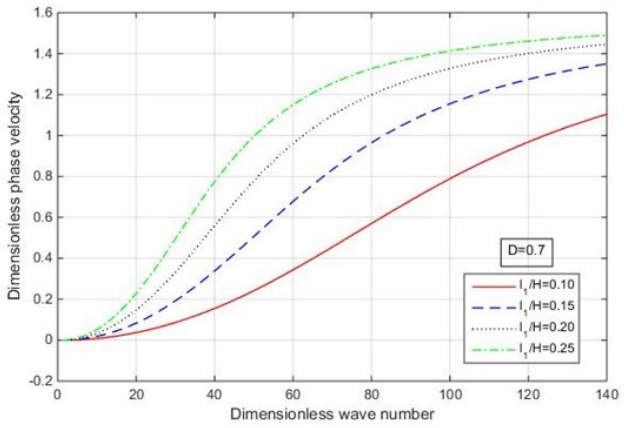


**Figure 11.** Dispersion curves for porosity factor $D = 0.7$ and the ratios $\frac{l_1}{H} = 0.10, 0.15, 0.20, 0.25$.

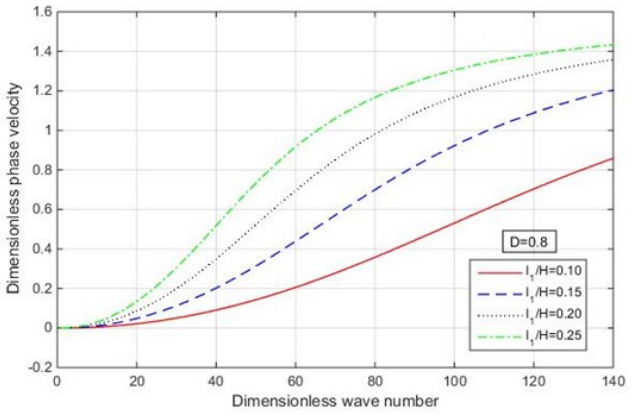


**Figure 12.** Dispersion curves for porosity factor $D = 0.8$ and the ratios $\frac{l_1}{H} = 0.10, 0.15, 0.20, 0.25$.

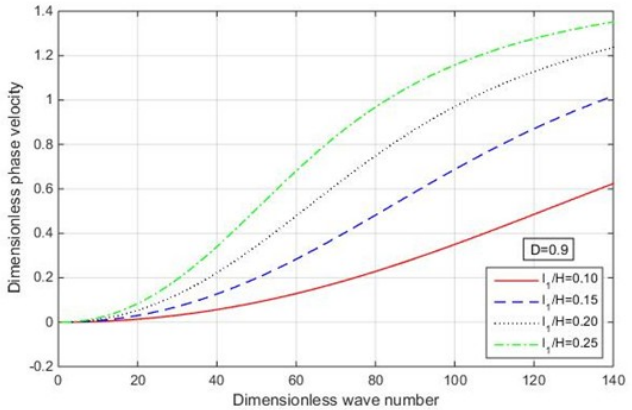


**Figure 13.** Dispersion curves for porosity factor $D = 0.9$ and the ratios $\frac{l_1}{H} = 0.10, 0.15, 0.20, 0.25$.

## 9 Conclusion

This study examines the propagation of shear waves in TIFSPL with a rigid upper surface boundary, situated above a heterogeneous elastic half-space. By using perturbation techniques, Biot's elasticity theory, and Fourier transformation methods, the dispersion relation for the model has been derived. It has been found that this dispersion equation is influenced by several factors, including the inhomogeneity parameter, wavenumber, porosity, phase velocity, the size and shape of the irregularity, and the layer height. The impact of various factors on non-dimensional phase velocity versus the non-dimensional wavenumber has been visualized graphically with MATLAB graphical tools. By analyzing the analytic and graphical results, the following main aspects of the study have been concluded:

- From Figure 2-5, an increment in the phase velocity is seen in both instances, firstly when the wavenumber is increasing and secondly when the ratio $(l_1/H)$ is increasing. It has also been noted that as the value of the inhomogeneity parameter $q$ increases, the magnitude of phase velocity decreases.
- Figures 6-7 demonstrate that within a homogeneous half-space, as the anisotropy factor $C_1/C_5$ increases for distinct values of the ratio $(l_1/H)$, it leads to an increment in phase velocity.
- Figures 8-9 examine that in a non-homogeneous half-space, an increase in the anisotropy factor $C_1/C_5$ for different values of the ratio $(l_1/H)$ also increases the phase velocity.
- Figures 8-9 conclude that as the heterogeneity parameter increases, the phase velocity slightly decreases.
- Figures 10-13 show that the phase velocity decreases as an increment in the porosity factor $(D)$, while a higher ratio $(l_1/H)$ value results in an increment in phase velocity. Additionally, crossing points are observed when the non-dimensional wavenumber is near 10 to 15.

Hence, it is determined that the layer's phase velocity is altered by factors including the wavenumber, inhomogeneity parameter, porosity, and the ratio $l_1/H$. These results are valuable for researchers in seismology, solid mechanics, and geophysics, particularly those studying wave propagation.

The findings of this study provide valuable insights into the geophysical behavior of shear waves in complex layered media. The combined effects of anisotropy, porosity, and triangular-shaped interface irregularity are found to significantly influence the dispersion characteristics and phase velocity of shear waves. Specifically, anisotropy and the depth or shape of interface irregularities tend to increase the SH-wave phase velocity, while higher porosity and material inhomogeneity lead to its reduction. These interactions emphasize the necessity of simultaneously considering multiple physical parameters when analyzing seismic-wave dispersion in realistic geological environments. In sedimentary basins and porous fault zones, neglecting the coupled influence of anisotropy, porosity, and interface geometry may result in biased velocity estimates and misinterpretation of subsurface conditions. Furthermore, the study reveals that the geometry of the interface, such as triangular irregularities, can cause branch crossings or noticeable shifts in dispersion curves, directly affecting seismic inversion outcomes and subsurface imaging accuracy. The theoretical framework developed here offers a robust foundation for improving seismic data interpretation and modeling of wave propagation in anisotropic and porous media. Incorporating these coupled effects into modeling and inversion strategies such as those used in ambient noise tomography or surface-wave surveys can lead to a more realistic characterization of subsurface structures. Future work could extend the present analysis to include attenuation mechanisms and perform comprehensive numerical simulations for complex basin geometries to further validate the theoretical predictions.

## Nomenclature

- M1: Transversely isotropic fluid-saturated porous layer.

- M2: Heterogeneous elastic half-space
- H: Height of porous layer
- $u_i$: Components of displacement vector for a solid in medium M1
- $U_i$: Components of displacement vector for a fluid in medium M1
- $\sigma_{ij}$: Components of stress tensor per unit area in medium M1
- $C_m$: Material constants used in the porous layer for $m = 1, 2, \ldots, 8$
- $\rho_s$, $\rho_\phi$: Mass densities for solid, liquid medium respectively
- $\phi$: Porosity of the porous layer
- $2s$: Maximum width of the irregularity
- $l_1$: Maximum depth of the irregularity
- $d$: Distance of source causing irregularity along $z$-axis
- $\tau_{ij}$: Components of the stress tensor in medium M2
- $v_i$: Components of the displacement vector in medium M2
- $\lambda, \mu$: Lame's coefficients
- $\delta_{ij}$: Kronecker delta
- $k$: Wavenumber
- $\omega$: Angular velocity
- $\mu_0, \rho_0, q$: Arbitrary constants
- $\Omega$: Dimensionless frequency
- $c_G$: Velocity of shear waves
- $t$: Time dependent variable
- $c$: Common wave velocity

## Appendix A

The definitions used in Section 5 and in the dispersion derivation:

$$\zeta_1^2 = \alpha_1 + i\,\alpha_2, \qquad \alpha_1 = \frac{F\omega^2}{c_G^2}, \qquad \alpha_2 = \frac{R\omega^2}{c_G^2}, \tag{.1}$$

$$F(\omega) = \frac{1 + \Omega^2\gamma_{22}C'}{1 + (\Omega\gamma_{22})^2}, \qquad R(\omega) = -\frac{(C' - \gamma_{22})\Omega}{1 + (\Omega\gamma_{22})^2}, \tag{.2}$$

$$C' = \gamma_{11}\gamma_{22} - \gamma_{12}^2, \qquad \gamma_{ij} = \frac{\rho_{ij}}{\rho}, \tag{.3}$$

$$c_G^2 = \frac{C_5}{D}, \qquad \Omega = \frac{\rho\,\omega}{b_{11}}, \qquad D = \rho_{11} - \frac{\rho_{12}^2}{\rho_{22}}, \tag{.4}$$

The wavenumbers and related quantities:

$$\chi_1^2 = \frac{C_1}{C_5}\Big(\frac{\zeta_1^2}{C_1} - k^2\Big), \tag{.5}$$

$$\chi_2^2 = k^2 - \frac{\omega^2}{\beta_0^2}, \qquad \beta_0^2 = \frac{\mu_0}{\rho_0}, \tag{.6}$$

$$\chi = \frac{1}{2}\Big(q + \sqrt{q^2 + 4\chi_2^2}\Big). \tag{.7}$$

Fourier transform definitions used in the analysis:

$$v_2^0(z,\eta) = \int_{-\infty}^{\infty} v_2^0(z,x)\, e^{-i\eta x}\, dx, \tag{.8}$$

$$v_2^0(z,x) = \frac{1}{2\pi}\int_{-\infty}^{\infty} v_2^0(z,\eta)\, e^{i\eta x}\, d\eta. \tag{.9}$$

## Appendix B

This appendix reproduces and organizes the coefficients $A_1, A_2, A_3, A_1^0, A_2^0, A_3^0$, $R(k)$, $E_1(k)$, $E_2(k)$, and the Fourier transforms of $h(x)$ used in the derivation.

**Coefficients $A_1$, $A_2$, $A_3$ and first-order corrections.**

$$A_2 = \frac{4\mu_0 e^{-\chi d}}{R(k)}, \tag{.10}$$

$$A_1 = \frac{4\mu_0 e^{-\chi d}\tan\chi_1 H}{R(k)}, \tag{.11}$$

$$A_3 = \frac{2e^{-\chi d}\big(\mu_0\chi\tan\chi_1 H - C_5\chi_1\big)}{\chi\, R(k)}, \tag{.12}$$

and the first-order (in $\epsilon$) coefficients:

$$A_1^0 = \frac{\tan\chi_1 H\,[\,E_2(k) - \mu_0\chi E_1(k)\,]}{R(k)}, \tag{.13}$$

$$A_2^0 = \frac{E_2(k) - \mu_0\chi E_1(k)}{R(k)}, \tag{.14}$$

$$A_3^0 = \frac{E_2(k)\tan\chi_1 H + \chi_1 C_5 E_1(k)}{R(k)}. \tag{.15}$$

where

$$R(k) = \mu_0\chi\tan\chi_1 H + C_5\chi_1. \tag{.16}$$

**Definitions of $E_1(k)$ and $E_2(k)$:**

$$E_1(k) = h(x)\big(A_2\chi_1 + A_3\chi - 2e^{-\chi d}\big), \tag{.17}$$

$$E_2(k) = h(x)\big(C_5\chi_1^2 A_1 + \mu_0\chi^2 A_3 + 2\mu_0\chi e^{-\chi d}\big) + i\eta h(x)\big(-A_1C_1 + \tfrac{2}{\chi}\mu_0 e^{-\chi d} + \mu_0 A_3\big). \tag{.18}$$

**Fourier transform of the irregularity function $h(x)$.**

$$\bar{h}(\lambda) = \int_{-\infty}^{\infty} h(x) e^{-i\lambda x}\, dx, \tag{.19}$$

$$h(x) = \frac{1}{2\pi}\int_{-\infty}^{\infty} \bar{h}(\lambda) e^{i\lambda x}\, d\lambda, \tag{.20}$$

and the derivative transform

$$h'(x) = -\frac{i}{2\pi}\int_{-\infty}^{\infty} \lambda\,\bar{h}(\lambda) e^{i\lambda x}\, d\lambda. \tag{.21}$$

**Definitions used in $g(k)$ and $E$ integrals.**

$$B_2 = A\chi_1^2 C_5 - \mu_0\chi\big(A_2\chi_1 - 4e^{-\chi d}\big), \tag{.22}$$

$$B_3 = -\lambda k\big[A_1 C_1 - \mu_0\big(A_3 + \tfrac{2}{\chi}e^{-\chi d}\big)\big], \tag{.23}$$

**Definition of $y(k)$ used in the dispersion condition:**

$$y(k) = 4\Big(C_5\chi_1^2 \tan\chi_1 H - \mu_0\chi\chi_1 + R(k)\chi\Big). \tag{.24}$$

## Appendix C

This appendix reproduces the expressions used to obtain the complex dispersion relation.

$$P_1 = \left[\frac{1}{C_5}\Big(\frac{Fc^2}{c_G^2} - C_1\Big) + \frac{i}{C_5}\frac{Rc^2}{c_G^2}\right]^{1/2}, \tag{.25}$$

$$P_2 = \frac{1}{2}\Big(Q + \sqrt{Q^2 + 4\Big(1 - \frac{c^2}{\beta_0^2}\Big)}\Big). \tag{.26}$$

**The complex root splitting and $k_1, k_2$:**

$$P_1 = k_1 + ik_2 \quad \text{(so } k_1, k_2 \text{ are real part and imaginary part of } P_1\text{)}. \tag{.27}$$

**Explicit expressions for $k_1$ and $k_2$:** Starting from

$$P_1 = \sqrt{A + iB}, \qquad P_1 = k_1 + ik_2,$$

where

$$A = \frac{1}{C_5}\left(\frac{F(\omega)\,c^2}{c_G^2} - C_1\right), \qquad B = \frac{1}{C_5}\left(\frac{R(\omega)\,c^2}{c_G^2}\right),$$

the real and imaginary parts of $P_1$ are obtained as

$$k_1 = \sqrt{\frac{\sqrt{A^2+B^2}+A}{2}}, \qquad k_2 = \sqrt{\frac{\sqrt{A^2+B^2}-A}{2}}.$$

$$A = \frac{1}{C_5}\left[\frac{c^2}{c_G^2}\left(\frac{1+\Omega^2\gamma_{22}C'}{1+(\Omega\gamma_{22})^2}\right) - C_1\right], \tag{.28}$$

$$B = -\frac{1}{C_5}\left[\frac{c^2}{c_G^2}\left(\frac{(C'-\gamma_{22})\,\Omega}{1+(\Omega\gamma_{22})^2}\right)\right]. \tag{.29}$$

Hence, the explicit formulae for $k_1$ and $k_2$ (equivalently $K_1$ and $K_2$) are:

$$k_1 = \sqrt{\frac{\sqrt{\left[\frac{1}{C_5}\left(\frac{c^2}{c_G^2}\frac{1+\Omega^2\gamma_{22}C'}{1+(\Omega\gamma_{22})^2} - C_1\right)\right]^2 + \left[\frac{1}{C_5}\frac{c^2}{c_G^2}\frac{(C'-\gamma_{22})\,\Omega}{1+(\Omega\gamma_{22})^2}\right]^2} + \frac{1}{C_5}\left(\frac{c^2}{c_G^2}\frac{1+\Omega^2\gamma_{22}C'}{1+(\Omega\gamma_{22})^2} - C_1\right)}{2}}, \tag{.30}$$

$$k_2 = \sqrt{\frac{\sqrt{\left[\frac{1}{C_5}\left(\frac{c^2}{c_G^2}\frac{1+\Omega^2\gamma_{22}C'}{1+(\Omega\gamma_{22})^2} - C_1\right)\right]^2 + \left[\frac{1}{C_5}\frac{c^2}{c_G^2}\frac{(C'-\gamma_{22})\,\Omega}{1+(\Omega\gamma_{22})^2}\right]^2} - \frac{1}{C_5}\left(\frac{c^2}{c_G^2}\frac{1+\Omega^2\gamma_{22}C'}{1+(\Omega\gamma_{22})^2} - C_1\right)}{2}}. \tag{.31}$$

These explicit forms guarantee that the dispersion relation can be evaluated directly in numerical routines without relying on implicit complex-square-root operations.

**Final expressions for $L_r$ and $L_i$:**

$$L_r = \frac{[\,2l_1kk_1(k_1^2C_5 + C_5k_2^2 + \mu_0P_2^2) \;-\; \mu_0P_2k_1\,]\,[\,C_5 - 2C_5l_1P_2k + 2l_1\mu_0P_2k\,]}{[\,2l_1kC_5(k_1^2 - k_2^2) + \mu_0P_2(2l_1kP_2 - 1)\,]^2 + (4kk_1k_2l_1C_5)^2}, \tag{.32}$$

$$L_i = \frac{-[\,2l_1kk_2(k_1^2C_5 + C_5k_2^2 - \mu_0P_2^2) + \mu_0P_2^2\,]\,[\,C_5 - 2C_5l_1P_2k + 2l_1\mu_0kP_2\,]}{[\,2l_1kC_5(k_1^2 - k_2^2) + \mu_0P_2(2l_1kP_2 - 1)\,]^2 + (4kk_1k_2l_1C_5)^2}. \tag{.33}$$

## Appendix D: Additional explicit definitions and porosity mapping

For convenience and reproducibility of numerical computations we explicitly state the porosity mapping and a few dimensionless relations used in the numerical section.

**Biot mass coefficients and porosity mapping**

$$\rho_{11} + \rho_{12} = (1-\phi)\rho_s, \tag{.34}$$

$$\rho_{12} + \rho_{22} = \phi\rho_f, \tag{.35}$$

$$\rho = \rho_s + \phi(\rho_f - \rho_s). \tag{.36}$$

The parameter $D$ that appears in $c_G^2 = C_5/D$ is defined by

$$D = \rho_{11} - \frac{\rho_{12}^2}{\rho_{22}}. \tag{.37}$$

If the numerical choice is $\rho_{12} = 0$ (used in manuscript numeric examples), then

$$D = \rho_{11} = (1-\phi)\rho_s, \qquad D_1 = \frac{D}{\rho_s} = 1 - \phi. \tag{.38}$$

Hence the non-dimensional porosity parameter values $D_1 = 0.6, 0.7, 0.8, 0.9$ used in plots correspond to physical porosities $\phi = 0.4, 0.3, 0.2, 0.1$ respectively.

## Declarations

**Competing interests:** The authors declare that there have no financial or personal conflicts of interest that may have affected the research findings discussed in this study.
**Funding:** No external funding received for this research work.
**Data availability statements:** Data may be available upon reasonable request from the corresponding author.

## References

[1] M. A. Biot, Theory of propagation of elastic waves in a fluid-saturated porous solid. II. Higher frequency range. J. Acoust. Soc. Am. (1956). https://doi.org/10.1121/1.19085241

[2] M. A. Biot, Mechanics of incremental deformations. John Willey and Sons, New York, (1966).

[3] Z. Koneczak, The propagation of Love waves in a fluid-saturated porous anisotropic layer. Acta Mechanica. (1989). https://doi.org/10.1007/BF01187260

[4] P.M. Shearer, Introduction to seismology. Cambridge university press. (2019).

[5] D. Gubbins, Seismology and Plate Tectonics. Cambridge University Press, Cambridge. (2003).

[6] A.E.H. Love, Some Problems of Geodynamics: Being an Essay to which the Adams Prize in the University of Cambridge was Adjudged in 1911. University Press. (1911).

[7] W. M. Ewing, , W. S. Jardetzky, F. Press, and A. Beiser, Elastic waves in layered media. Physics Today, 10(12), 27-28. (1957).

[8] K. F. Graff, Rayleigh and lamb waves, pp. 1–649. New York, NY: Dover. (1991).

[9] J. Achenbach, Wave propagation in elastic solids. Elsevier. (2012).

[10] A. Chattopadhyay, and B.K. Kar, Love waves due to a point source in an isotropic elastic medium under initial stress. International Journal of Non-Linear Mechanics, 16(3-4), 247-258. (1981).

[11] S.C. Dutta, P.K. Das, and P. Sengupta, Seismic behavior of irregular structure, Structural Engineering International, 27(4), 526-545, (2017).

[12] A. Chattopadhyay, S. Gupta, A.K. Singh, and S.A. Salim, Propagation of shear waves in an irregular magnetoelastic monoclinic layer sandwiched between two isotropic half-spaces. International Journal of Engineering Science and Technology, 1(1), 228-244, (2009). https://doi.org/10.4314/ijest.v11i.58082

[13] A. Chattopadhyay, S. Gupta, V.K. Sharma, and P. Kumari, Propagation of shear waves in viscoelastic medium at irregular boundaries. Acta Geophysics, 58(2), 195-214 (2010). https://doi.org/10.24788/s11600-009-0060-3

[14] P. Alam, S. Kundu, and S. Gupta, Dispersion study of SH-wave propagation in an irregular magneto-elastic anisotropic crustal layer over an irregular heterogeneous half-space. Journal of Klug and University-Science, 30(3), 301-310. (2018). https://doi.org/10.1016/j.jklgus.2016.11.007

[15] R. Kant, S.K. Vishwakarma, and T.R. Panigrahi, Influence of irregular geologies and inhomogeneity on SH-wave propagation. Acta Mechanics, 231(5), 1821-1836. (2020). https://doi.org/10.1007/s00707-019-02589-2

[16] Y.S. Wang, and Z.M. Zhang, Propagation of Love waves in a transversely isotropic fluid-saturated porous layered half-space. J. Acoust. Soc. Am. 103(2), 695-701. (1998). https://doi.org/10.1121/1.421196

[17] S. Gupta, S.K. Vishwakarma, D.K. Majhi, and S. Kundu, Possibility of Love wave propagation in a porous layer under the effect of linearly varying directional rigidities. Applied Mathematical Modelling, 37(10-11), 6652-6660. (2013). https://doi.org/10.1016/j.apm.2013.01.008

[18] S. Kundu, S. Gupta, A. Chattopadhyay, and D.K. Majhi, Love wave propagation in porous rigid layer lying over an initially stressed half-space. International journal of applied physics and mathematics, 3(2), 140, (2013). https://doi.org/10.77621/JAPM.2013.V3.193

[19] R. Kumar, and A. Saini, Influence of Parabolic Irregularity, Inhomogeneity, Initial Stress, and Anisotropy on Love Wave Propagation. *Mechanics of Solids*, 59(3), 1443-1458. (2024)

[20] R.Kumar, D.K. Madan, and J. S. Sikka, Effect of Irregularity and Inhomogeneity on the Propagation of Love Waves in Fluid Saturated Porous Isotropic Layer. Journal of Applied Science and Technology, 22 (8-2), 18-21 (2016)

[21] S. Manna, S. Kundu, and S. Gupta, Effect of reinforcement and inhomogeneity on the propagation of Love waves. International Journal of Geomechanics, 16(2), 04015045. (2016). https://doi.org/10.1051/(ASCDC)A14943-562.0000517

[22] R. Kumar, A. Saini, S. Sharma, and Sunaina. Investigating SH-wave dynamics in anisotropic media with triangular surface irregularities and initial stress influence. In IET Conference Proceedings CP912, 38, 433-438, (2024).

[23] A. Saini, and R. Kumar, Analysis of Love Waves in an intially stressed transversely isotropic porous layer over heterogeneous half space with parabolic irregularity. Journal of Vibrational Engineering and Technology, 12(7), 7373-7386. (2024).

[24] A. Chattopadhyay, S. Gupta, V. Sharma, and P Kumari, Effects of irregularity and anisotropy on the propagation of shear waves. International Journal of Engineering, Science and Technology, 2(1), 116-126, (2010). https://doi.org/10.4314/ijest.v21i.59100

[25] S.K. Samal, and R. Chattaraj, Surface wave propagation in fiber-reinforced anisotropic elastic layer between liquid saturated porous half space and inflorn liquid layer. Acta Geophysics, 59(3), 470-482, (2011). https://doi.org/10.24788/s11600-011-0002-8

[26] R. Kumar, D.K. Madan, and J. S. Sikka, Shear wave propagation in multilayered medium including an irregular fluid saturated porous stratum with rigid boundary. Advances in Mathematical Physics, 1, 163505. (2014). https://doi.org/10.11550/104165360

[27] S. Kundu, S. Gupta, and S. Manna, SH-type waves dispersion in an isotropic medium sandwiched between an initially stressed orthotropic and heterogeneous semi-infinite media. Meccanica, 49(3), 749-758, (2014). https://doi.org/10.1007/s11012-013-9896-8

[28] S. Kundu, P. Alam, and S. Gupta, Shear waves in magneto-elastic transversely isotropic (MTI) layer bonded between two heterogeneous elastic media. Mechanics of Advanced Materials and Structures, 26(5), 407-415, (2019). https://doi.org/10.1080/15376494.2017.1400614

[29] S. Gupta, S. K. Das, and S. Pramanik, Impact of Irregularity, initial stress, porosity, and corrugation on the propagation of SH wave. International Journal of Geomechanics, 21(2), 04020245, (2021). https://doi.org/10.1051/(ASCDC)A14943-562.0001882

[30] R. Kumar, S. Sharma, and S. Chandel, Impact of triangular irregularity, material heterogeneity and initial stress on the propagation of shear waves in a transversely isotropic porous layer. International Journal of Applied Mechanics and Engineering, 30(2), 89-104. (2025).

[31] S. Sharma, and R. Kumar, Analyzing the Role of Triangular Surface Irregularity and Initial Stress on SH-Wave Behavior in Multilayer Anisotropic Media. In 2024 International Conference on Emerging Technologies and Innovation for Sustainability (EmergIN) (pp. 473-478). (2024).

[32] R.K. Poonia, N. Bashtiya, and V. Kaliraman, Influence of Rigidity, Irregularity and Initial Stress on Shear Waves Propagation in Multilayered Media. Journal of Solid Mechanics. 12(4), 713-728, (2020).

[33] R. Kumar, and A. Saini, Effect of anisotropy, inhomogeneity and porosity on love wave propagation through fluid-saturated porous layers in irregular layered media. The European Physical Journal Plus, 139(12), 1-20, (2024). https://doi.org/10.1140/epjp/s13360-024-05914-5

[34] S. Sharma, and R. Kumar, Love Wave Propagation in a Homogeneous Thermoelastic Layer over a Non-Homogeneous Half-Space with Triangular Irregularity. Mech. Solids (2025). https://doi.org/10.1134/S0025654425602162

[35] A. Saini and R. Kumar, Love Wave Propagation in an Isotropic Thermoelastic Layer With Rigid Boundary Lying Over a Nonhomogeneous Elastic Half-Space, Mathematical Methods in the Applied Sciences (2025): 1–10, https://doi.org/10.1002/mma.70117.

[36] A. Gaba, A. Rani, and N. Kumar, Static Deformation in an Initially Stressed Magneto-Elastic Transversely Isotropic Half-Space affected by Imperfect Interface. Palestine Journal of Mathematics, 14(3), 111-125, (2025).

[37] K. Singh, M. Kashyap, and A. A. Pir, Effects of Memory-Dependent Heat Transfer and Impedance Boundary Conditions onWave Propagation in a Micropolar Thermoelastic Material. Palestine Journal of Mathematics, 14. (2025).

[38] H.F. Willis, LV. A formula for expanding an integral as a series. The London, Edinburgh, and Dublin Philosophical Magazine and Journal of Science (1948). https://doi.org/10.1080/14786444808521694

## Author information

Ravinder Kumar, Department of Mathematics, University Institute of Sciences, Chandigarh University, Mohali-140413, Punjab, India.
E-mail: ravinderpoonia25@gmail.com

Suraj Sharma, Department of Mathematics, University Institute of Sciences, Chandigarh University, Mohali-140413, Punjab, India.
E-mail: bhardwajsuraj070@gmail.com

Ananya Goyal, Department of Mathematics, University Institute of Sciences, Chandigarh University, Mohali-140413, Punjab, India.
E-mail: gananya201@gmail.com

Received: 2025-03-11
Accepted: 2025-11-11